Thermal cycle around the critical point of carbon dioxide under reduced gravity

P. Guenoun, B. Khalil, and D. Beysens
Service de Physique de l'Etat Condensé, Centre d'Etudes de Saclay, F-91191 Gif-sur-Yvette CEDEX, France

Y. Garrabos, F. Kammoun, and B. Le Neindre
Laboratoire d'Ingéniérie des Matériaux et des Hautes Pressions, Institut Galilée-Université Paris Nord, Avenue Jean-Baptiste Clément, F-93430 Villetaneuse, France

B. Zappoli
Centre National d'Etudes Spatiales, 18 av. Edouard Belin, F-31055 Toulouse CEDEX, France
(Received 10 December 1991)

In order to investigate the different aspects of the transport of heat in the absence of gravity, we performed a thermal cycle close to and around the critical point of CO_2 at critical density. Reduced gravity was provided during a 6-min flight of a sounding rocket. A cell has been designed which allows surface and bulk phenomena to be distinguished. Special optical devices are used to observe the sample and measure locally temperature and density. We also present experiments under Earth's gravity at a few mK from the critical temperature (T_c). Convection patterns are observed which correspond to Grashof numbers as large as a few 10^4. The thermal cycle of the experiment in weightlessness starts at $T_c+2.5$ mK, where we study the relaxation of the perturbations caused by liftoff: fluid flows, density and temperature gradients. We then investigate the effect of a quench from $T_c+2.3$ to $T_c+1.3$ mK, and the expected mechanism of heat transport by the "Piston effect" (PE) is experimentally evidenced. In particular, we observe homogeneous thermalization, with a time of thermalization less than a few seconds. We compare this time with a number of theoretical estimations. During thermalization, density and temperature gradients are not affected by the PE and are seen to relax diffusively. We perform then a quench at $T_c-0.8$ mK. We observe the onset of phase separation, making a clear visualization of the PE. Thereafter, spinodal decomposition occurs, followed by the growth of a bicontinuous pattern of gas and liquid domains. After a last quench back to $T_c+2.0$ mK, we still observe the PE in spite of the presence of density gradients. These gradients are seen to relax by diffusion.

PACS number(s): 05.70.Jk, 44.10.+i, 66.10.Cb

I. INTRODUCTION

The transport of heat in dense pure fluids classically involves the mechanisms of convection, diffusion, and radiation. This paper provides unambiguous experimental evidence of a fourth mechanism, the "Piston effect" (PE), which is related to the compressibility of the fluid. A number of predictions by Kassoy [1], Onuki, Hao, and Ferrel [2], Zappoli *et al.* [3,4], and Boukari *et al.* [5] have pointed out the relevance of this mode of heat transport in compressible fluids. Straub and Nitsche [6] have considered in contrast a mechanism which involves only diffusive processes. Our recent numerical simulations of the entire set of Navier-Stokes equations for a van der Waals gas [4] have helped us to understand the physical basis of the PE. When heated near a wall, the diffusive boundary layer of a compressible fluid can expand, generating an acoustic wave which travels back and forth in the system as a piston. The thermal conversion of this wave is, in turn, able to heat the fluid uniformly after a few acoustic time steps, resulting in an increase of pressure. Although the PE should be relevant in an ideal gas [7], it is near the gas-liquid critical point, where the fluid compressibility diverges, that it should be more pronounced [4]. It is in the vicinity of this point that all the studies have been performed up to now.

Earlier anomalies of conductivity measurements in ^{3}He and ^{3}He-^{4}He mixtures have been recently successfully reanalyzed by Behringer, Onuki, and Meyer [8] in terms of the PE. These measurements have been performed in a specially designed cell and sufficiently far from the critical point to make the gravity effects as small as possible. Recent experiments of light transmissivity in xenon a few mK above the critical point by Boukari *et al.* [9] also report a fast and bulk thermalization. However, their cell did not minimize the gravity effects.

The possible effects of the convections driven by the Earth's gravitational field are a common factor to all ground-based experiments. Indeed, the Rayleigh and Grashof numbers become extremely large in the vicinity of the critical point, as a consequence of the diverging compressibility of the fluid and the very slow thermal diffusion ("critical slowing down"). This means that even minute temperature gradients in the fluid can generate convective instabilities, as we show below. As a matter of fact, recent simulations of the transport in an ideal gas by Sutrisno and Kassoy [10] show that gravity affects the transport even on the acoustic time scale. These flows are, in turn, responsible for the fast and bulk character of the thermalization of the fluid. Because these charac-

teristics are the same as those resulting from the PE, and because the PE was not suspected until very recently, the very short temperature equilibrium times of compressible fluids have been attributed to convective flows only.

Consequently, we think that experiments where the gravitational field is suppressed are mandatory to give clear and unambiguous demonstration of the PE transport of heat. Two observations have already been performed under weightlessness that support the existence of the PE. In a pioneering experiment with SF_6, Nitsche and Straub [11] did not observe the expected dramatic slowing down of the heat transport when crossing the critical point. The same kind of observation has been performed recently by Klein *et al.* [12], also with SF_6. These experiments, however, were not specially designed to study the PE, and mixed phase separation and thermalization. Also, the bulk character of the thermalization has not been reported.

In order to circumvent the above problems, we have carried out an experiment under weightlessness (TEXUS 25 [13]). In principle, convective flows should be negligible, since the gravity level is reduced by at least four orders of magnitude. In addition, the direction of the residual acceleration randomly fluctuates with time at such a high frequency that possible residual convective flows are prevented from reaching a large spatial scale.

Our experimental system consists of a transparent cell filled with carbon dioxide (CO_2) at critical density ($\rho=\rho_c=467.8$ kg m^{-3}). The cell is mounted in a high-precision thermostat and follows a thermal cycle at constant density close to its critical temperature ($T\approx T_c=304.14$ K). Light transmissivity measurements through the cell enable temperature and density inhomogeneities to be obtained at each point of the sample. A comb-shadow technique is used to measure the density gradients independently [14].

In the following sections (II–IV) we give more details about the experimental setup and the procedure which enables the thermal behavior of the fluid to be extracted. Section V is concerned with the thermal equilibrium process under Earth's gravity and the convective flows which can be generated in the fluid. The main results are discussed in Sec. VI, where we show that the PE is the dominant mechanism of heat transport when a thermal quench is performed. We demonstrate that the temperature equilibration occurs homogeneously in the bulk of the sample and is much faster than a pure diffusive behavior. This result is significant, since pure diffusion would lead to equilibration times of the order of 1 week for $T-T_c\approx 1$ mK, whereas the PE thermalizes the sample in about a few seconds or less. It is also observed that the inhomogeneities in density are not affected by the PE and relax diffusively.

II. EXPERIMENT

The experimental cell (Fig. 1) is made of a stainless steel parallelepiped and two windows. The internal volume is a cylinder (10.106 mm internal diameter, $e=7.48$ mm thickness), with two sapphire windows (10.030 mm external diameter, 9.025 mm length) epoxied to the steel wall using their cylindrical surface. The cell is filled with CO_2 (L'Air Liquide, of quality better than 99.998%) at the density of 467.83 kg m^{-3}, with an accuracy better than 0.01%. After a temperature quench in the thermostat, heat may diffuse from the windows leading to a change in light transmittancy (see below), which would give rise to an erroneous interpretation of a bulk thermalization. In order to discriminate between surface and bulk effects, an annealed gold thread (0.3-mm diameter) is set in the central part of the sample cell. It is thermally discoupled from the cell by alumina tubes and PTFE foils (polytetrafluoroethylene) and is coupled to the thermostat. Because alumina is a poor conductor compared to gold (the ratio of conductivity is of order 15) and because the windows are off from the body of the cell by a 0.038 mm layer of insulating epoxy, the windows are heated up more slowly than the gold thread and the inner walls of the cell. Thus diffusion, if it occurs, would be observed clearly around the thread by a change of light transmissivity during the first seconds which follow the thermostat quench (this is explained below in more detail).

The cell is mounted in a high-precision copper thermostat which can be cooled and heated rapidly using a Peltier element. The temperature is measured by a stabilized YSI thermistor loaded into the copper wall of the thermostat. Temperature stability is within 0.1 mK and spatial temperature gradients are less than 0.1 mK cm^{-1}. There exists, however, a weak coupling between the temperature of the electronic regulation box and the set point temperature. From calibration experiments it is possible to correct this bias, which corresponded for the flight experiment to a linear decrease in temperature of 0.085 mK/min. Temperature quenches are performed at a rate of 0.3 mK/s. The minimum temperature step is 0.2 mK. The cell is illuminated by a white light parallel beam. A plane of order 0.2 mm thickness, located close to the exit window, is imaged on a CCD video camera. Between the cell and the camera lens, a comblike array of threads is

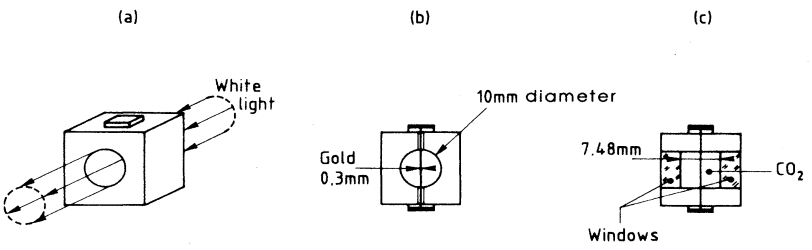

FIG. 1. Sketch of the experimental cell. (a) General view, (b) front view, (c) side view. The gold thread in the middle of the cell is thermally insulated from the body and is directly connected to the thermostat.

set. The deformation of its shadow on the CCD camera gives a measure of the refractive index gradients from which we can deduce the density gradients in the sample [14]. This comb does not cover all the field of view in order to analyze the light transmitted through the sample [see the window of analysis W_b in Fig. 2(c)]. The whole setup is loaded in a sounding rocket whose ballistic trajectory gives access to 6 min of reduced gravity. The residual acceleration is lower than 10^{-4} times the terrestrial gravity and is randomly oriented. The parameters of the experiment and the video signal are sent to the ground control station where they are recorded [super video high standard (SVHS)]. Unfortunately, the video signal was noisy in the time interval (105–140 s). Because our quantitative analysis of the video images involves the measurement of the background noise, no data from this time period will be reported. Remote control is used to command the temperature changes from the ground.

III. THERMAL CYCLE

In the vicinity of T_c the fluid is hypercompressible and gravitational effects are important. The fluid is stratified in density (Fig. 3), and, after a temperature step, cells of convection are clearly visible (Fig. 4) even in the most favorable configuration to prevent convection. Before liftoff, the value of T_c is determined within 0.2 mK and the cell temperature is set 2.5 mK above T_c. After the launch and before the microgravity (μg) period, the rocket is spun at a rate of 120 rpm. Despinning, which occurs at the start of the μg period about 57 s after liftoff, generates flows in the cell. These flows stop about 20 s later (Fig. 2). The relaxation of the density gradients caused by the Earth's gravity, the launch acceleration, and the spinning of the rocket are studied at nearly constant temperature ($T_c+2.4$ mK) during the first 90 s of μg. Then, to investigate the heat transport by the PE and its possible influence on the density gradients, a thermal quench of 1 mK (quench 1) is performed leaving the system at $T_c+1.3$ mK. After 90 s, the fluid is quenched from $T_c+1.2$ mK to $T_c-0.8$ mK (quench 2). Here the temperature equilibration process couples with phase separation. The resulting complex phenomenon is the object of a separate paper [15]. In the following we only report the results concerning thermal equilibration. After 120 s, the last phase of the experiment consists of the return of the system back to the one-phase region at $T_c+2.0$ mK (quench 3). This phase ends 60 s later by the reentry of the payload in the atmosphere.

IV. TEMPERATURE MEASUREMENTS

From the transmissivity coefficient $\mathcal{T}=I_t/I_0$, where I_t (I_0) is the transmitted (incident) light intensity, one infers the sample turbidity

$$\tau=-(1/e)\ln(\mathcal{T}) . \quad (1)$$

Here e is the optical thickness of the sample. Turbidity is caused by fluctuations in refractive index (n) which scatter light. Another source of light attenuation is the refraction caused by refractive index inhomogeneities,

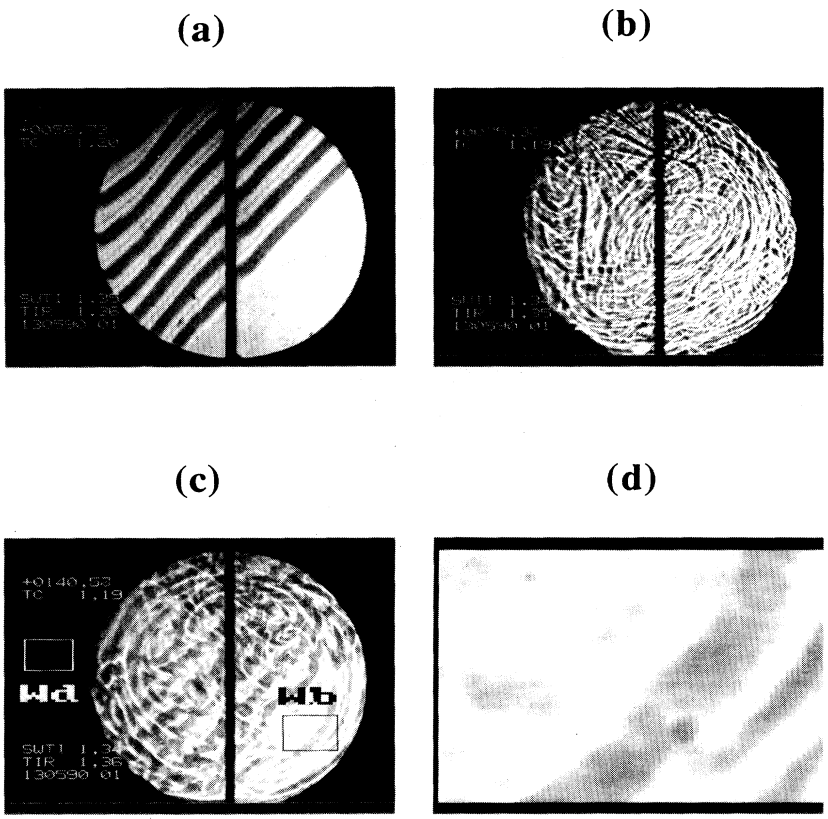

FIG. 2. Video image (front view) of the sample cell. (a) At $t=56.73$ s just before the microgravity period, when the rocket is still spinning. The centrifugational acceleration is of order 2 g and is directed left, perpendicular to the vertical thread. The deviation of the comb and the region of larger turbidity indicate that the density gradients are directed parallel to the acceleration. (b) At $t=75.30$ s, when the flows induced by despinning have just stopped. Density gradients with a periodicity of order 0.3 mm are clearly visible. (c) At $t=140.58$ s, just before quench from $T_c+2.3$ mK to $T_c+1.3$ mK (quench 1). It is clear that the gradients have relaxed if one compares this picture to (b). The quantitative analyses have been performed in two windows: (i) a window W_d in a nonilluminated region which enables the light transmissivity of the sample to be determined, and (ii) a window W_b in the cell for the density gradient evolution. An enlarged view of W_b is shown in (d).

whose influence is analyzed below.

The mean amplitude of the n fluctuations, and thus the turbidity, is related to the isothermal compressibility K_T within a corrective factor $G(k\xi)$. This factor accounts for the interference corrections when the correlation length ξ becomes comparable to the light wave vector k:

$$\tau \propto K_T G(k\xi) . \tag{2}$$

The turbidity τ can then be considered as a local measurement (at the scale of the light wavelength) of K_T. For a fluid at critical density, the temperature dependence of τ is well established and the transmitted light can be used as a local probe of the fluid temperature. Straightforward algebra [16,17] shows that τ is an asymptotic logarithmic function of the relative temperature $T-T_c$. A numerical estimate shows that, within less than 1%, a simple linear relationship between the relative temperature and the light transmissivity is valid a few mK around T_c,

$$T-T_c \propto \mathcal{T} . \tag{3}$$

However, the density of the sample varies locally. These density gradients are made visible [Fig. 2(b)] because they deform the shadow of the comb and, in the region where this comb is not present, modify the light transmissivity. These inhomogeneities are not randomly distributed in the window of analysis W_b [Figs. 2(c) and 2(d)], but rather they are mostly distributed radially, with a periodicity $\Lambda_R \approx 0.3$ mm. An order of magnitude of the density variation in the radial direction (R) can be evaluated to be $d\rho/dR = \delta\rho/\Lambda_R$, where $\delta\rho$ represents the amplitude of the density deviation with respect to ρ_c. The mean value of the gradient along the direction (X) of light propagation,

$$\langle d\rho/dR \rangle_X = (1/e)\int_0^e (d\rho/dR)\,dX , \tag{4}$$

can be estimated by the deformation of the shadow of the comb. Just before quench 2, the gradients measured by the comb correspond to a local density difference $\delta\rho/\rho_c \approx 10^{-2}$.

The gradients modify the image brightness because the propagation of light is modified. A first-order expansion

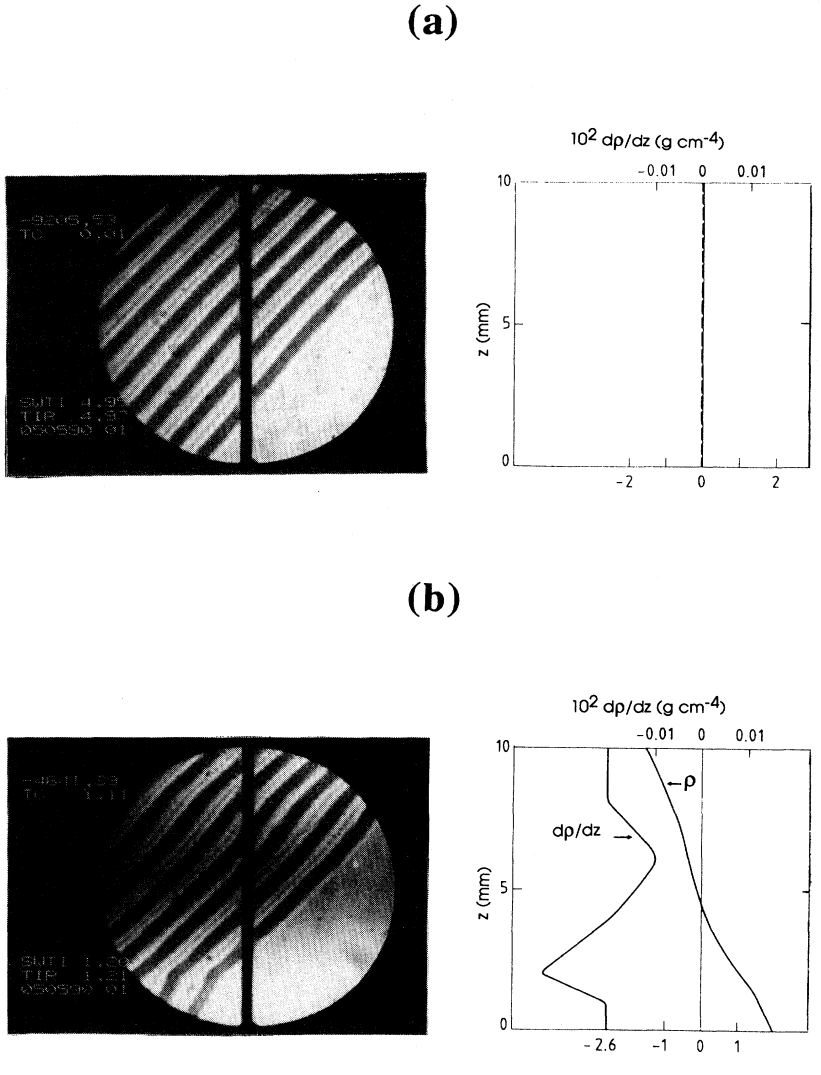

FIG. 3. Measurement of the density gradients induced by gravity by using the comb-shadow technique [14]. Gravity is directed downwards. (a) Reference pattern at $T-T_c=77$ mK. (b) At $T-T_c=2$ mK, CO_2 is compressed under its own weight. The density gradient is directed along z. The density profile is determined by numerical integration of the gradient and by assuming the cell to be filled at critical density.

analysis shows that the change of light intensity is connected to the second derivative of ρ that we approximate along X as

$$\delta\mathcal{T} \propto \langle d^2\rho/dR^2 \rangle_X \propto \delta\rho\Lambda_R^{-2} . \quad (5)$$

The change can be either a lowering or an increase of intensity, as shown by the histogram of W_b in Fig. 5. This histogram shows schematically a central peak corresponding to the critical density and two lateral peaks due to the density inhomogeneities. The same change of intensity can be also observed in a simple situation where the variation of ρ is due to the Earth's gravity and is directed along the Z-vertical direction. In Fig. 3-c of Ref. [14], according to the sign of $d^2\rho/dZ^2$, one can observe on the same sample either a dark line (near the bottom) or a bright line (near the top).

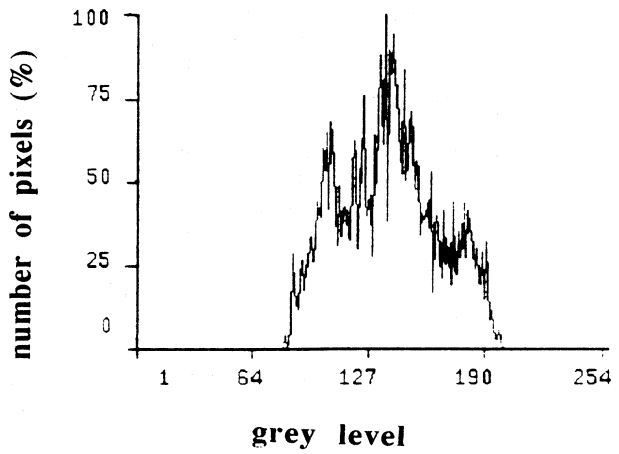

FIG. 5. Histogram of the grey levels in the window W_b of Fig. 2(d). The variance of this histogram is related to the amplitude of the density gradients. The number of pixels is expressed in percentage.

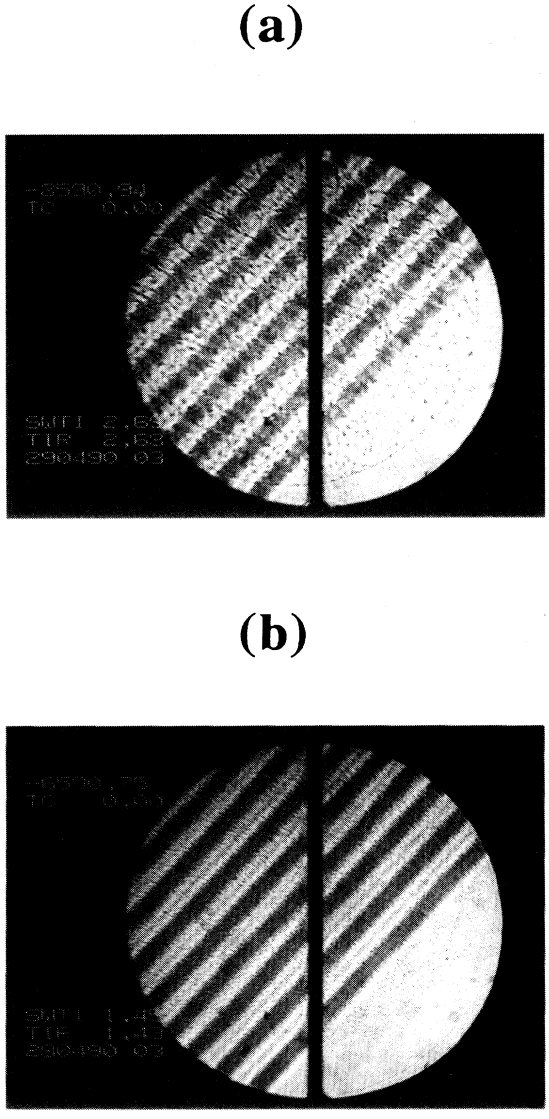

FIG. 4. Convective structures observed with gravity directed perpendicular to the plane of the figure. (a) When quenching the sample from $T-T_c=48$ mK to 28 mK. (b) The same structures are observed closer to T_c, i.e., with a quench from T_c+8 mK to T_c+3 mK. Here the contrast is weaker.

The influence of a deviation $\delta\rho$ from ρ_c leads to two main consequences on temperature measurements: (i) the relationship Eq. (3) can be altered, (ii) the transmissivity can vary because of refraction effects. Let us analyze these two phenomena in detail.

A. Influence of density gradients on turbidity

The existence of a deviation $\delta\rho$ first modifies the phase separation temperature by an amount δT_{cs}. This amount can be determined by the shape of the coexistence curve, whose equation for CO_2 is [18]

$$|\rho^{+,-}-\rho_c|/\rho_c = 1.6[(T_c-T)/T_c]^{0.325} . \quad (6)$$

Here $\rho^{+,-}$ are the densities of liquid and gas phases. For relative deviations of order $|\delta\rho/\rho_c| \approx 10^{-2}$, as it is observed just before the quench through T_c, the shift is of order $\delta T_{cs} \approx 5\times10^{-6}$ K. This shift can be neglected.

A second effect is to locally modify the temperature T by the amount δT according to

$$\delta T = \delta\rho/\rho_c\alpha_p , \quad (7)$$

where $\alpha_p = [(1/\rho)(\partial\rho/\partial T)_p]$ is the isobaric coefficient of thermal expansion. Just before quench 1 from 2.3 to 1.3 mK from T_c where $|\delta\rho/\rho_c| \approx 5\times10^{-2}$, the α_p value is $\alpha_p \approx 2.5\times10^3$ K^{-1}, which leads to $\delta T \approx 2\times10^{-5}$ K, a value which is also negligible.

The last effect of the density variation is to change the amplitude of K_T by an amount δK_T. According to the K_T isothermal variations [18], $\delta K_T/K_T \approx \delta\rho/\rho_c \approx \delta\tau/\tau$, or $\delta T/(T-T_c) \approx e\tau(\delta\rho/\rho_c)$. The numerical evaluation at +2.3 mK from T_c just before quench 1, where $\tau \approx 200$ m^{-1} and $|\delta\rho/\rho_c| \approx 5\times10^{-2}$, leads to $\delta\mathcal{T}/\mathcal{T} = \delta T/(T-T_c) \approx 7\times10^{-2}$, that is, $\delta T = 0.15$ mK. After quench 1, closer to T_c, $\delta T/(T-T_c)$ becomes 2×10^{-2}, corresponding to a temperature change of 0.02 mK. These

values are less than the scatter of the data and we will neglect the variations of τ with $\delta\rho$. Equation (3), where temperature and transmittivity are linked by a simple relation of proportionality can thus be applied, even in the presence of density gradients.

The measurement of the light transmissivity is performed by analyzing the video image. For this purpose the gain $\mathcal{G}$ of the CCD camera has to be known. This gain is continuously adjusting in order to avoid saturation of the video signal. We have developed [19] a method to determine $\mathcal{G}$ from an analysis of the image background, such as the window W_d in Fig. 2(c). The method is based on the determination of the histogram of the grey levels of the dark pixels (background signal) whose variance $\mathcal{V}_d$ appears to be proportional to the gain of the camera:

$$\mathcal{G} \propto \mathcal{V}_d \ . \tag{8}$$

We will see in the next section that the average video signal $\langle i \rangle$ represents the light transmissivity at the critical density, and is therefore proportional to temperature according to the above analysis.

B. Density-gradient evolution

The evolution of the density gradients, and then of the density deviation $\delta\rho$, can be deduced from the deformation of the shadow of the comb. We use this method to determine the amplitude of $\delta\rho$ at a particular time (just before quench 2). Because analyzing the comb is very time consuming, we instead analyze how the histogram of the grey levels in the window W_b evolves. This histogram (Fig. 5) is symmetrical in shape and shows schematically a central peak corresponding to the average (critical) density, and two lateral peaks resulting from the $\delta\rho$-induced light defocusing (dark pixels) and focusing (bright pixels). As time elapses, the density inhomogeneities relax and the histogram becomes bell shaped. The distribution variance appears therefore as an easy measurement of the density relaxation. For the particular situation of window W_b, where inhomogeneities correspond to parallel stripes separated by the distance $\Lambda_R \approx 0.3$ mm, one can approximate the amplitude of the density variation as $\delta\rho \approx \Lambda_R^2 \langle d^2\rho/dR^2 \rangle_X$.

In Ref. [19], a calibration has allowed the relation between the grey level i and the corresponding light intensity I to be expressed as

$$I \propto i^2/\mathcal{G} \propto i^2/\mathcal{V}_d \ . \tag{9}$$

The average grey level value $\langle i \rangle^2$ is thus proportional to the transmissivity $\mathcal{T}$ at critical density. From (3) it follows that

$$T - T_c \propto \langle i \rangle^2/\mathcal{V}_d \ . \tag{10}$$

Figure 5 shows that the histogram of the grey levels in W_b is not a simple Gaussian function. We nevertheless approximate the relation between the transmissivity variation $\delta\mathcal{T}$ and the variance $\mathcal{V}_b = (\delta i)^2$ by simply taking the derivative of Eq. (9) around the grey histogram mean intensity $\langle i \rangle$:

$$\delta\mathcal{T} \propto \langle i \rangle \mathcal{V}_b^{1/2}/\mathcal{V}_d \ . \tag{11}$$

From Eqs. (5), (9), (10), and (11) one obtains the simple formulas

$$T - T_c = a \langle i \rangle^2/\mathcal{V}_d \ , \tag{12}$$

$$\delta\rho = b \langle i \rangle \mathcal{V}_b^{1/2}/\mathcal{V}_d \ . \tag{13}$$

Here a and b are the proportionality factors that are determined by imposing the average value $T - T_c = 2.4$ mK between the times 65 and 100 s, just at the beginning of the experiment, and $\delta\rho/\rho_c = 10^{-2}$ just before quench 2.

V. CONVECTIVE HEAT TRANSPORT UNDER THE GRAVITY FIELD

Because of the particular geometry which is involved in this experiment, it is difficult to infer from theory only the precise importance of the convective heat transport. Therefore, a number of experiments have been performed with the setup under the Earth's gravity field.

The dimensionless number which gives a measure of the relative importance of viscous and inertial effects versus buoyancy is the Grashof number (Gr) [20]. This number is written as

$$\mathrm{Gr} = g\alpha_p \Delta T L^3/\nu^2 \ , \tag{14}$$

where g is the gravitational acceleration, ΔT is the temperature difference which extends over the length L in the fluid, and ν is the kinematic viscosity. It follows from Eq. (14) that Gr is very sensitive to the value of L, a quantity difficult to estimate *a priori* without performing experiments.

Figure 4(a) is a photograph of the cell in Earth's gravity during a thermal quench from $T - T_c = 48$ mK to 28 mK. The gravity vector is directed parallel to the smallest dimension of the cell which is the most stable situation. Convective structures are clearly evidenced, however. A similar observation [Fig. 4(b)] can be made as close as $T - T_c = 3$ mK after a 5-mK quench. These structures appear as soon as temperature in the thermostat is lowered and evolve during the transient, i.e., a few seconds, which is the time necessary for the thermostat to reach a constant temperature. Note that these patterns are very similar to those obtained during directed solidification [21]. The convections have the same qualitative features as the PE, i.e., they accelerate and homogenize the fluid temperature.

The spatial scale of these structures is roughly $L = 0.15$ mm at $T - T_c = 3$ mK. This makes possible an estimation of the order of magnitude of Gr for quench 1. At $T - T_c \approx 1$ mK, $\alpha_p = 7 \times 10^3$ K^{-1}, $\nu = 9 \times 10^{-8}$ m^2 s^{-1}, and ΔT is of order 1 mK. With $L \approx 0.15$ mm, this leads to $\mathrm{Gr} \approx 3 \times 10^4$. One can estimate the error in L to be within a factor of 3. Such a large value of Gr suggests that in experiments performed under terrestrial gravity it is very difficult to prevent the influence of convections. In contrast, Gr is reduced by a factor of 10^4 in our experiment. This low value and the fact that residual accelerations are randomly oriented give us confidence that the

convective flows are negligible during the whole thermal cycle.

VI. RESULTS UNDER REDUCED GRAVITY AND DISCUSSION

A. Heat transport in the one-phase region (quenches 1 and 2)

The main result of this experiment is concerned with the very fast heat transport equilibration time as shown in Fig. 6. The typical diffusion time over distance d (cell half-thickness $d=e/2$) is

$$t_D=(D_T)^{-1}d^2 . \tag{15}$$

Here $D_T=2.2\times10^{-11}$ m^2 s^{-1} is the thermal diffusivity at $+1.3$ mK from T_c. The typical diffusion time appears to be more than 1 week at this temperature. In contrast, the experimental time t_E for quench 1 is of about 20 s.

Another striking observation is the absence of any noticeable transmitted light gradient around the gold thread and the cell walls during and after the quenches. As expected [2–6], the PE gives rise to a homogeneous thermalization, at least during the 40-ms scanning time of a video picture. This observation becomes particularly clear for quench 2 (Fig. 7) where the sample temperature crosses T_c. Here the nucleation of small droplets of liquid and vapor makes the sample opalescent and enables the thermalization process to be detected.

Although the data can be fit to an exponential function, the scatter of the data does not allow an unambiguous determination of the relaxation profile to be determined. It is possible, however, to compare the order of

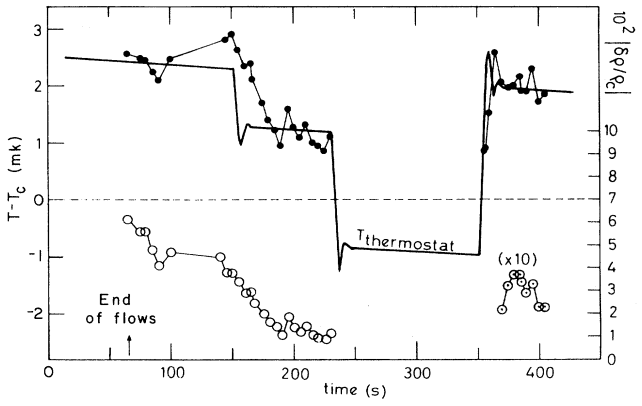

FIG. 6. Temperature profile in the cell (●) with respect to time. The solid line is the temperature in the thermostat close to the cell. The open circles (○) correspond to the density inhomogeneities for $t<250$ s, whose scale is on the right. The dotted circles (⊙) correspond to the data for $t>350$ s, whose scale is expanded by a factor of 10. The measurements started after the flow in the sample has stopped. No information can be inferred when the temperature is below T_c because the fluid is then separating into two phases. The results are striking: whereas the density inhomogeneities relax diffusively, temperature equilibrates much faster, thanks to the thermocompressible transport of heat (the typical time for thermalization by diffusion is of order 1 week at 1 mK from T_c).

magnitude of t_E with a number of typical times involved in different mechanisms. But before considering the heat transport in the fluid, one has to estimate heat diffusion in the thermostat and in the cell body. The thermostat has first to reach the final temperature, which takes about $t_1\approx4$ s as measured by the thermistor. Neglecting the time of diffusion in the copper block, heat has to diffuse from the cell outer wall to the cell inner wall, i.e., on a length of order 10 mm. With a thermal diffusivity of 7×10^{-6} m^2 s^{-1} for the stainless steel used here, the typical diffusion time is $t_2\approx14$ s. Then the total equilibration time (t_1+t_2) for the solids is of order of t_E. The accuracy of the above calculation is within a few seconds, which means that the true fluid thermal equilibration time (t_T) is less than a few seconds.

Let us consider the different time scales which are involved in the fluid thermalization. The acoustic time t_A should correspond to the relaxation of the pressure in the cell at the end of the external temperature change. Here $t_A=e/2c\approx10$ μs, with $c\approx100$ m s^{-1} the sound velocity from [22] extrapolated at 1 mK from T_c. This very small time is out of the accessible range of the experiment.

Another small time is t_L associated with the development of a thermal diffusive boundary layer. Equilibration can be effective at least when the heat quantity in the layer has reached the quantity necessary to change the temperature of the fluid. According to Onuki, Hao, and Ferrel [2], such an equilibration time after a very rapid quench is

$$t_{L,O}=t_D/\gamma^2\propto(T-T_c)^{1.7} , \tag{16}$$

with γ the ratio of specific-heat coefficients at constant pressure and volume. As γ is very large close to the critical point, the above relation represents an enormous reduction in the time required for the fluid to come to thermalization. At $T_c+1.3$ mK, $\gamma\approx1.3\times10^5$, which gives $t_{L,O}\approx30$ μs. Another prediction for t_L can be deduced from the one-dimensional hydrodynamic analysis of a van der Waals gas by Zappoli [3],

$$t_{L,Z}\propto(T-T_c)^{3/2} . \tag{17}$$

The difference in the exponents of Eqs. (16) and (17) is caused by the difference between Ising and mean-field exponents. By using the numerical results obtained at $+10$ K from T_c [4], i.e., 22 s to reach 90% equilibration, and extrapolating them at $T_c+1.3$ mK thanks to Eq. (17), one obtains a typical time of 30 μs, the same value as from Eq. (16) (this equality is a mere coincidence). Anyway, both $t_{L,Z}$ and $t_{L,O}$ values can fit the data.

One can consider also a mass diffusion time t_M. A very first guess is to consider the self-diffusion coefficient D_{11}, whose value at T_c+1 mK can be estimated to be of the order of 10^{-8}–10^{-9} m^2 s^{-1}. In the considered temperature range it is approximately temperature independent and corresponds to a typical time of $t_M=100$–1000 s. This time does not agree with the experimental data. Straub and Nitsche [6], however, proposed another expression for t_M in a special situation where a hydrostatic pressure gradient is present, as under the Earth's gravity field:

$$t_M = \gamma t_L = t_D/\gamma \propto (T - T_c)^{0.5} . \quad (18)$$

This time is of order 5 sec at 1 mK from T_c. Although this time can be compared with our data, under zero gravity no pressure gradient should exist in the bulk.

Another limiting time entering in the process is the hydrodynamic time $t_H = e^2/4\nu \approx 160$ s, which measures the flow relaxation in the sample. The relaxation time of the despinning-induced flows is of order 20 s in this experiment; the factor-of-8 discrepancy with the calculation is presumably due to geometrical factors. According to the hydrodynamic theory of the PE, heating in the Navier-Stokes equation is due to the $\nabla(vp)$ term (v is the fluid velocity and p is pressure). Then the temperature evolution stops in the fluid when the flow due to the expansion of the boundary layer stops, that is, after the external temperature change has stopped and the flow is relaxed. This occurs for the typical time t_H. As a matter of fact, the equilibration time in the numerical simulation of Ref. [4] at $+10$ K from T_c is 22 s, which is still of order t_H. Then our results might also be understood in terms of relaxation of the flow velocity induced by the thermal expansion of the boundary layer. Note that the temperature variation of t_H is governed by ν, which varies only slightly in the neighborhood of T_c.

B. Heat transport in the two-phase region (quench 3)

The last quench has been performed in a sample which is phase separated into an interconnected pattern of vapor and liquid domains (Fig. 8) whose densities at $T - T_c = -1$ mK can be estimated to be 2.7% off critical according to Eq. (6). The temperature evolution has been determined for a window W_b' inside a single phase—a vapor droplet (we know it is a vapor domain because it does not wet the cell wall). Here the transmissivity follows Eq. (3). Thermalization is again homogeneous as seen from the homogeneous clearing up of the pattern. We attribute this clearing when entering the one-phase region to the relaxation of the smallest domains that scatter light very much. Its typical evolution is of tens of seconds, as above in the one-phase region. It is a striking demonstration that, although interfaces are present, the PE is still efficient in a very compressible diphasic fluid.

C. Density and temperature inhomogeneities

Another question was the investigation of the influence of the PE-induced flow on density and temperature inhomogeneities. Figure 6 shows the evolution of the density variations ($\delta\rho$) as deduced from the histogram of the grey levels of window W_b according to Eq. (13). One first notes that the amplitude of the density inhomogeneities at the beginning of the experiment ($6\times10^{-2}\rho_c$) corresponds to what was expected from a sample submitted to accelerations of several-g amplitude. From Fig. 6 it is clear that the density relaxation is not severely affected by quench 1 and that the time relaxation of the density is diffusive. This diffusion time is of order 100 s for the density inhomogeneities in the window of analysis W_b [Figs. 2(c) and 2(d)]. According to Eq. (15), where $d = \Lambda_R/2\pi$, the above time corresponds to the relaxation at $T_c + 1$

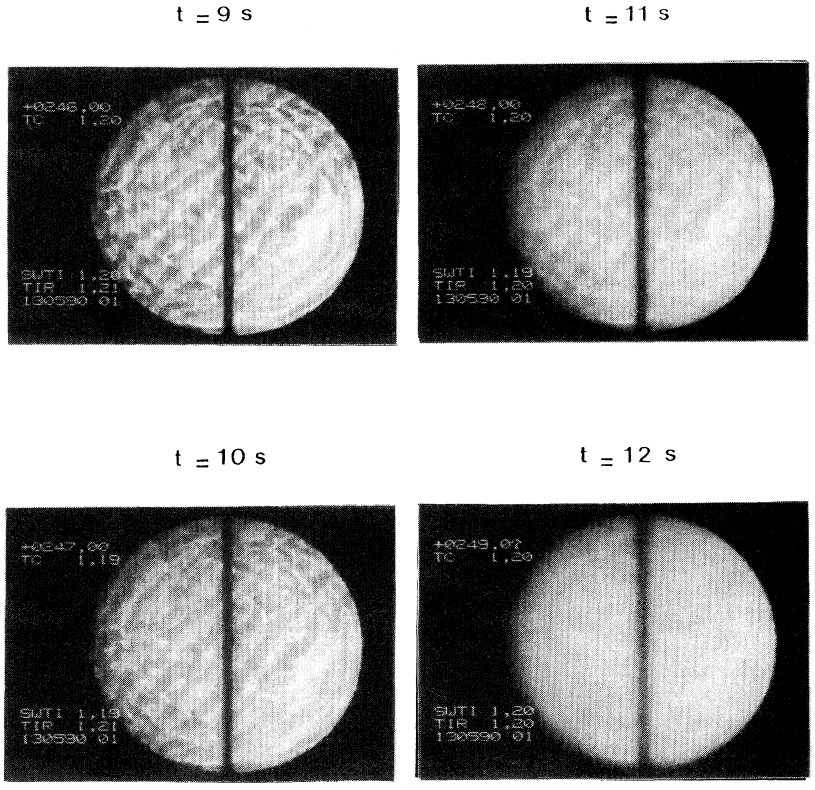

FIG. 7. Aspect of the sample cell after a quench from $T_c + 1.2$ mK to $T_c - 0.8$ mK (quench 2). The time is numbered after the thermostat has reached its equilibrium value. The cell opalescence is due to the onset of the phase separation and allows the crossing of T_c to be made visible. As expected, thermalization by the PE is homogeneous.

mK of periodic structures of wavelength $\Lambda_R \approx 0.3$ mm.

The relaxation of density inhomogeneities that results from the phase separation can also be determined after quench 3 back in the one-phase region by the same technique as above [Eq. (13)]. The window of analysis W_b' is located inside a vapor domain (see Fig. 8), in which tiny droplets of the other phase are present. These droplets can be attributed to the process of phase separation itself, as observed in liquid mixtures, or to the nucleation of new droplets induced by the temperature drift, of order 0.2 mK during the separation process. The evolution of the corresponding deviation is reported on Fig. 6. Only the data where the gradients of density are visible are reported ($t \geq 350$ s). Before thermalization, no gradients are apparent because the sample is very fuzzy, a phenomenon presumably resulting from the interaction of many small domains that cannot be resolved by the present optics. As PE thermalizes the sample, these small domains vanish by diffusion, which makes the sample look clearer. However, the largest domains are still present. They also vanish by diffusion. Then the peak in the time evolution of $\delta\rho$ can be understood as follows: first, thermalization that makes progressively visible in the window of analysis the largest gradients; second, relaxation by diffusion of these gradients. The time scale of this relaxation is of order 30 s. If one calculates the diffusion time from Eq. (15) at $T_c + 2$ mK for typical density inhomogeneities of period Λ' ($d = \Lambda'/2\pi$), this time corresponds to a diffusion process for $\Lambda' \approx 0.2$ mm, in agreement with the size of the structures seen in Fig. 8.

VII. CONCLUSION

What comes out of this study is the behavior of very compressible fluids in the absence of gravity effects. Density inhomogeneities are seen to relax by diffusion, a result of practical importance for any scientific and technical operation in space dealing with such very compressible fluids. Thermalization, however, can be ensured in a time much smaller than expected from thermal diffusion

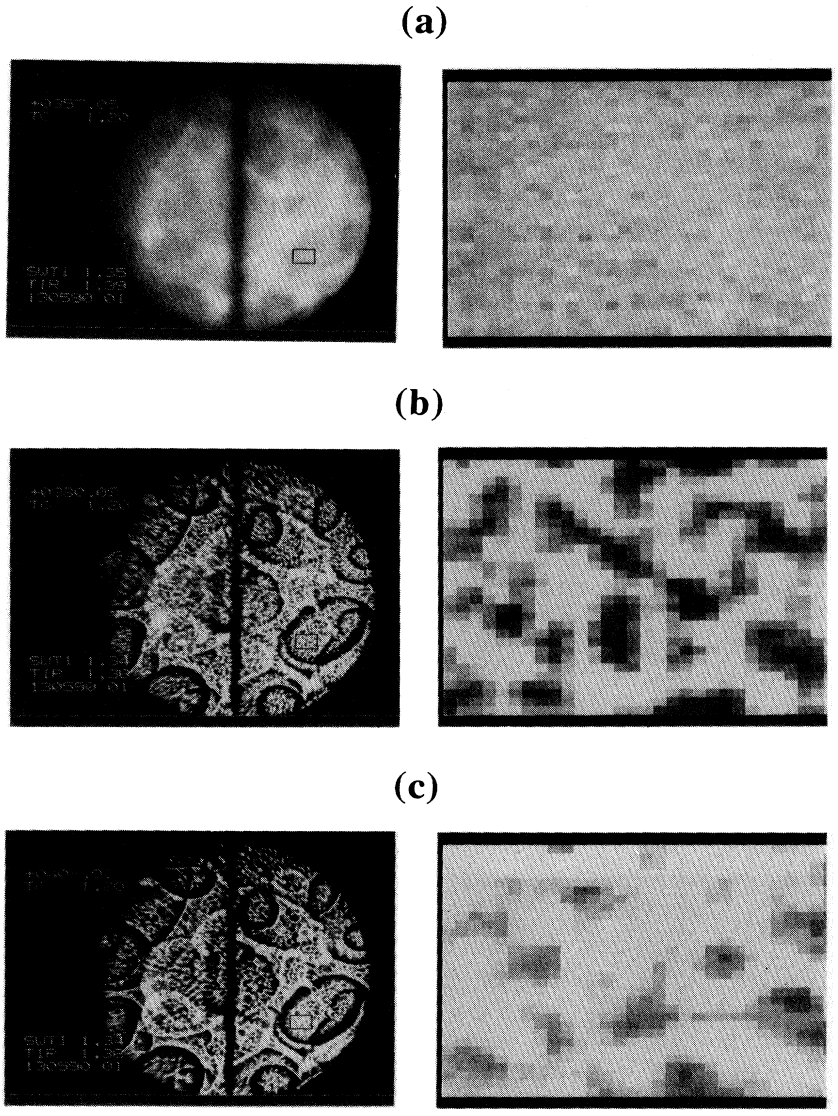

FIG. 8. Aspect of the sample cell after the temperature of the thermostat has been raised from $T_c - 1$ mK to $T_c + 2$ mK (quench 3). The window of analysis W_b' has been magnified on the right. (a) $t = 357.08$ s. The thermostat reaches the equilibrium value $T_c + 2$ mK. No gradient is visible. Thermalization by the PE starts. (b) $t = 380.08$ s. Gradients are now clearly evidenced (this picture corresponds to the peak of $\delta\rho/\rho_c$ in Fig. 6). These gradients are due to small vapor and liquid domains thermalized by the PE. They are not at equilibrium and relax by diffusion, as shown by (c). (c) $t = 405.08$ s, the latest time available before the reentry of the payload in the atmosphere.

only thanks to the PE. Since the theories that describe the thermalization predict quite different temperature behavior, a systematic temperature investigation would be very helpful. Because the coupling of gravitational flows with the PE is still an open problem, it seems doubtful that such experiments could lead to unambiguous results if performed under the Earth's gravity field.

ACKNOWLEDGMENTS

We thank P. Hede for help in the image analysis and M. Bonetti, R. F. Berg, R. W. Gammon, H. Meyer, M. Moldover, and J. Straub for useful comments and suggestions. This work has been partially supported by the Centre National d'Etudes Spatiales (Paris, France). The flight has been provided by the European Space Agency (Paris, France). The experiment module has been constructed by MBB ERNO (Bremen, Germany). We gratefully acknowledge the TEXUS team for its kind technical assistance. The Service de Physique de l'Etat Condensé is a Laboratoire de la Direction des Sciences de la Matière du Commissariat à l'Energie Atomique. The Laboratoire d'Ingéniérie des Matériaux et des Hautes Pressions is the UPR 1311 of the CNRS.

[1] D. R. Kassoy, SIAM **36**, 624 (1979).
[2] A. Onuki, H. Hao, and R. A. Ferrel, Phys. Rev. A **41**, 2255 (1990); A. Onuki and R. A. Ferrel, Physica A **164**, 245 (1990).
[3] B. Zappoli, Phys. Fluids A **4**, 1040 (1992).
[4] B. Zappoli, D. Bailly, Y. Garrabos, B. Le Neindre, P. Guenoun, and D. Beysens, Phys. Rev. A **41**, 2264 (1990); N. Djennaoui, F. Heraudeau, P. Guenoun, D. Beysens, and B. Zappoli, Acta Astronautica (to be published).
[5] H. Boukari, J. N. Shaumeyer, M. E. Briggs, and R. W. Gammon, Phys. Rev. A **41**, 2260 (1990).
[6] J. Straub and K. Nitsche (unpublished) and private communication.
[7] B. Zappoli and D. Bailly, Phys. Fluids A **10**, 1771 (1990).
[8] R. P. Behringer, A. Onuki, and H. Meyer, J. Low Temp. Phys. **81**, 71 (1990).
[9] H. Boukari, M. E. Briggs, J. N. Shaumeyer, and R. W. Gammon, Phys. Rev. Lett. **65**, 2654 (1990).
[10] Sutrisno and D. R. Kassoy, J. Eng. Math. (to be published).
[11] K. Nitsche and J. Straub, Naturwissenschaften **73**, 370 (1986); J. Straub and K. Nitsche (unpublished).
[12] H. Klein and B. Feuerbacher, Phys. Lett. A **123**, 183 (1987); H. Klein, G. Schmitz, and D. Woermann, Ber. Bunsenges. Phys. Chem. **92**, 870 (1988); H. Klein, G. Schmitz, and D. Woermann, Phys. Rev. A **43**, 4562 (1991).
[13] TEXUS 25 sounding rocket is a program of ESA (launch date: May 13, 1990).
[14] V. Gurfein, D. Beysens, Y. Garrabos, and B. Le Neindre, Opt. Commun. **85**, 147 (1991).
[15] Y. Garrabos, B. Le Neindre, P. Guenoun, B. Khalil, and D. Beysens, Europhys. Lett. **19**, 491 (1992).
[16] V. G. Puglielli and N. C. Ford, Jr., Phys. Rev. Lett. **25**, 143 (1970).
[17] J. H. Lunacek and D. S. Cannell, Phys. Rev. Lett. **27**, 841 (1971).
[18] R. Hocken and M. R. Moldover, Phys. Rev. Lett. **37**, 29 (1976); J. V. Sengers and M. R. Moldover, Phys. Lett. **66A**, 44 (1978).
[19] F. Kammoun, J. P. Astruc, D. Beysens, P. Hede, and P. Guenoun, Rev. Sci. Instrum. **63**, 7 (1992).
[20] D. J. Tritton, *Physical Fluid Dynamics* (Oxford University, London, 1988).
[21] D. C. Miller, in *Materials Processing in the Reduced Environment of Space,* edited by G. E. Rindon (Elsevier, New York, 1982), p. 373.
[22] P. C. Albright, T. J. Edwards, Z. Y. Chen, and J. V. Sengers, J. Chem. Phys. **87**, 1717 (1987).

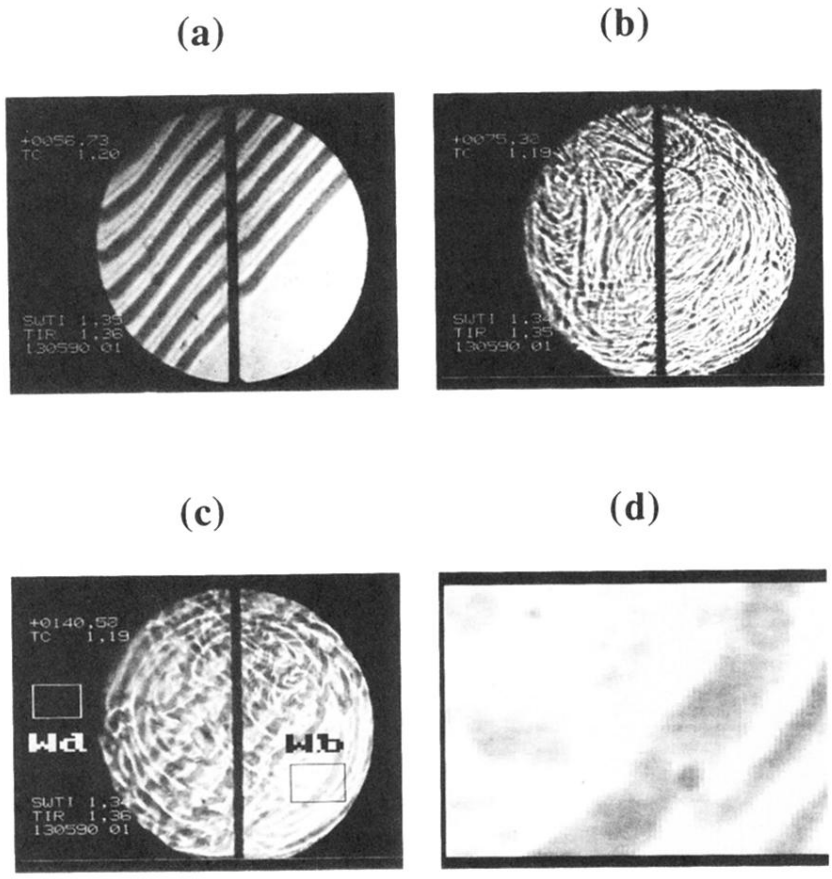

FIG. 2. Video image (front view) of the sample cell. (a) At $t=56.73$ s just before the microgravity period, when the rocket is still spinning. The centrifugational acceleration is of order 2 g and is directed left, perpendicular to the vertical thread. The deviation of the comb and the region of larger turbidity indicate that the density gradients are directed parallel to the acceleration. (b) At $t=75.30$ s, when the flows induced by despinning have just stopped. Density gradients with a periodicity of order 0.3 mm are clearly visible. (c) At $t=140.58$ s, just before quench from $T_c+2.3$ mK to $T_c+1.3$ mK (quench 1). It is clear that the gradients have relaxed if one compares this picture to (b). The quantitative analyses have been performed in two windows: (i) a window W_d in a nonilluminated region which enables the light transmissivity of the sample to be determined, and (ii) a window W_b in the cell for the density gradient evolution. An enlarged view of W_b is shown in (d).

(a)

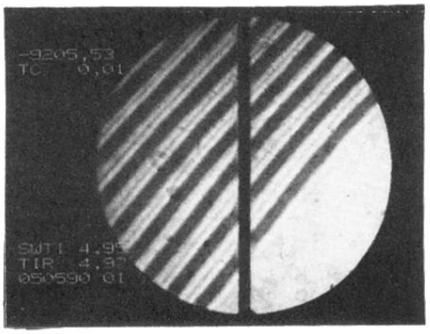

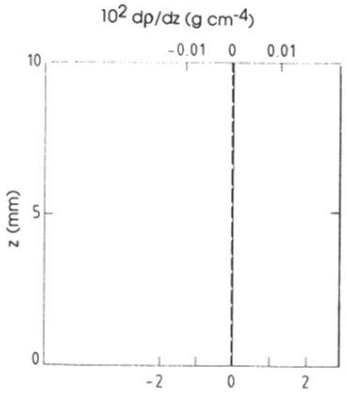

(b)

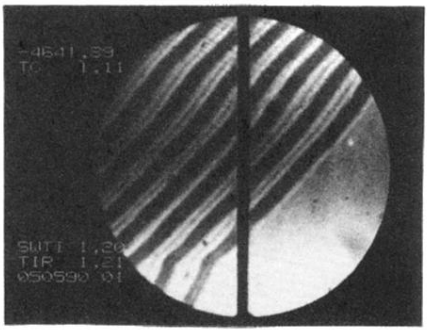

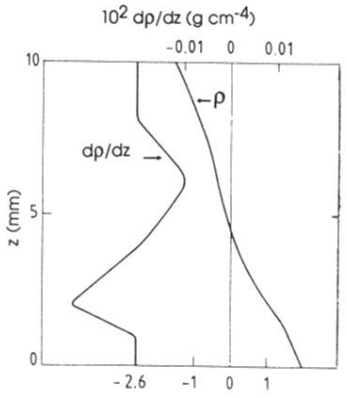

FIG. 3. Measurement of the density gradients induced by gravity by using the comb-shadow technique [14]. Gravity is directed downwards. (a) Reference pattern at $T-T_c=77$ mK. (b) At $T-T_c=2$ mK, CO_2 is compressed under its own weight. The density gradient is directed along z. The density profile is determined by numerical integration of the gradient and by assuming the cell to be filled at critical density.

(a)

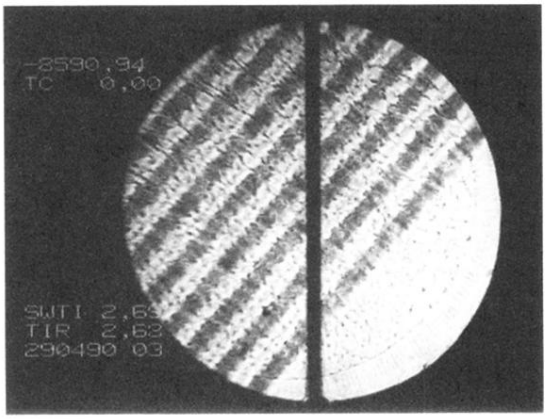

(b)

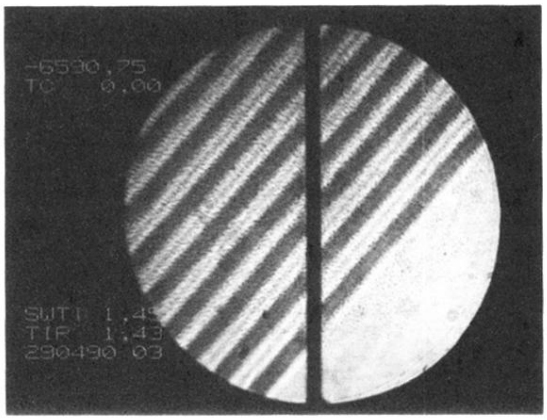

FIG. 4. Convective structures observed with gravity directed perpendicular to the plane of the figure. (a) When quenching the sample from $T-T_c=48$ mK to 28 mK. (b) The same structures are observed closer to T_c, i.e., with a quench from T_c+8 mK to T_c+3 mK. Here the contrast is weaker.

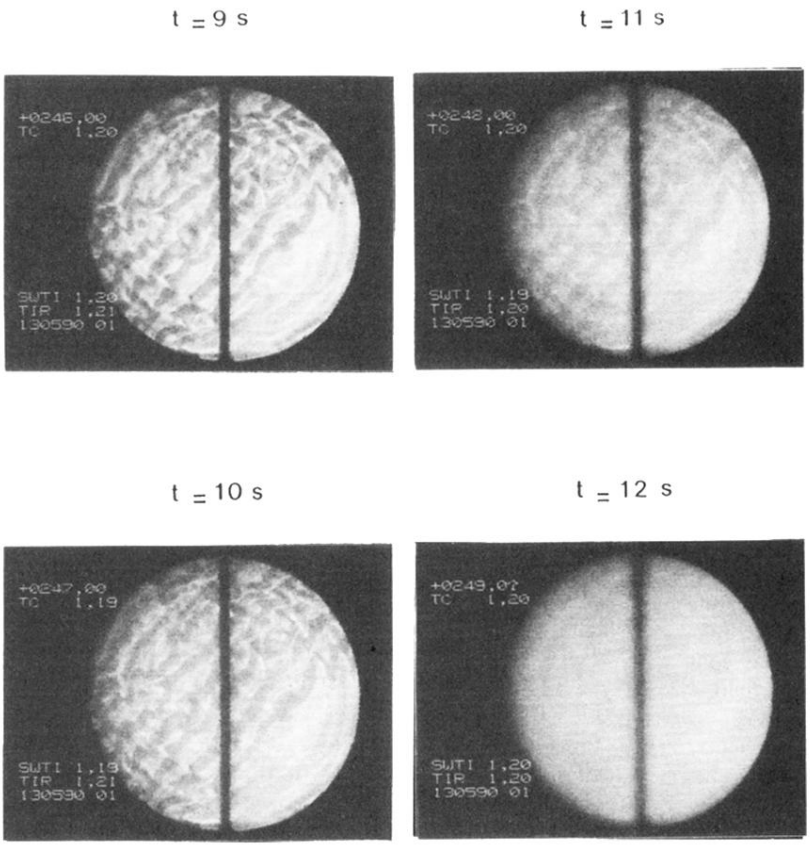

FIG. 7. Aspect of the sample cell after a quench from $T_c+1.2$ mK to $T_c-0.8$ mK (quench 2). The time is numbered after the thermostat has reached its equilibrium value. The cell opalescence is due to the onset of the phase separation and allows the crossing of T_c to be made visible. As expected, thermalization by the PE is homogeneous.

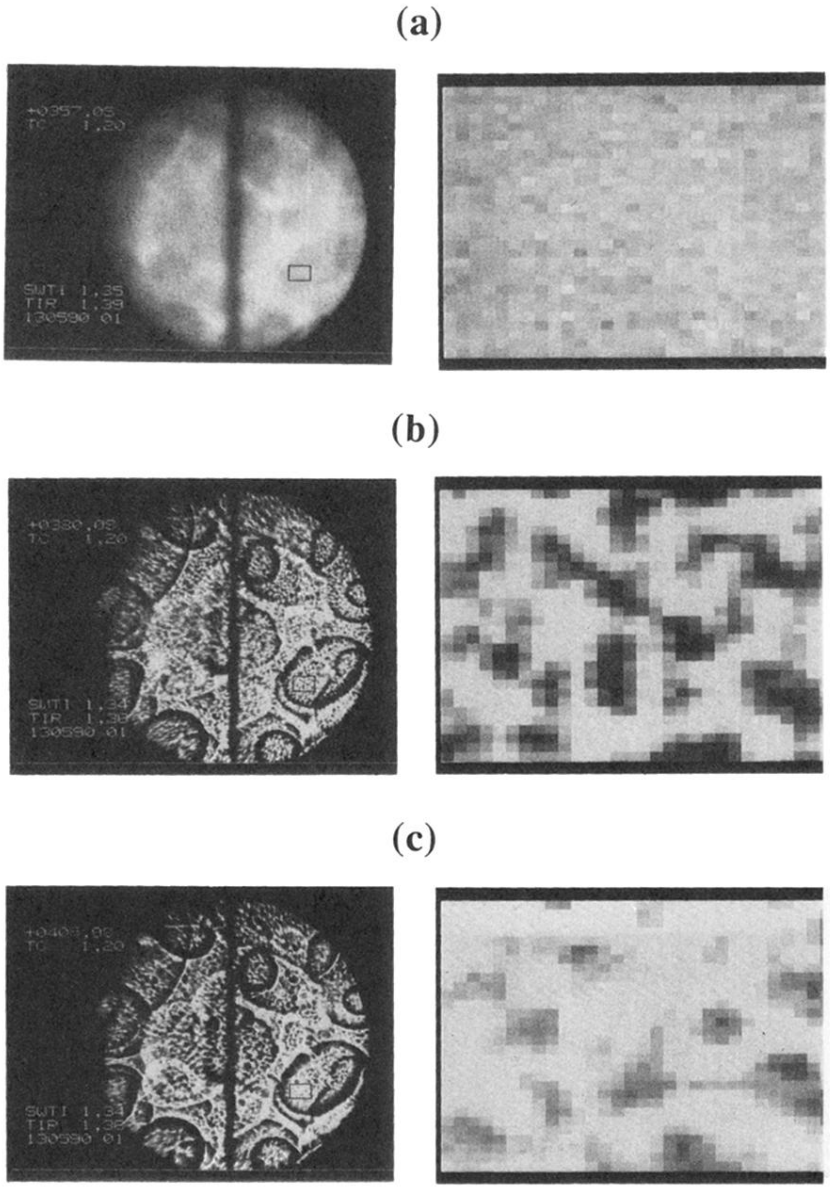

FIG. 8. Aspect of the sample cell after the temperature of the thermostat has been raised from $T_c - 1$ mK to $T_c + 2$ mK (quench 3). The window of analysis W_b' has been magnified on the right. (a) $t = 357.08$ s. The thermostat reaches the equilibrium value $T_c + 2$ mK. No gradient is visible. Thermalization by the PE starts. (b) $t = 380.08$ s. Gradients are now clearly evidenced (this picture corresponds to the peak of $\delta\rho/\rho_c$ in Fig. 6). These gradients are due to small vapor and liquid domains thermalized by the PE. They are not at equilibrium and relax by diffusion, as shown by (c). (c) $t = 405.08$ s, the latest time available before the reentry of the payload in the atmosphere.